JOURNAL OF APPLIED PHYSICS VOLUME 42, NUMBER 2 FEBRUARY 1971

Explosive Gas Blast: The Expansion of Detonation Products in Vacuum

THOMAS J. AHRENS
Seismological Laboratory, California Institute of Technology, Pasadena, California 91109
AND
CHARLES F. ALLEN
Stanford Research Institute, Menlo Park, California 94205
AND
ROBERT L. KOVACH
Department of Geophysics, Stanford University, Stanford, California 94305
(Received 18 May 1970; in final form 4 September 1970)

A series of 0.2- to 3-gm HNS charges were detonated in vacuums of 10^{-3} to 10^{-5} Torr. The resultant freely expanding, detonation product, gas blast achieves terminal velocities of 8 to 12 km/sec within 3 to 5 μsec after the detonation wave arrives at the free surface. Measured pressure profiles display rise times to maximum stagnation ("reflected shock") pressure varying from $\sim$30 μsec, 20-cm away from a 2.6-gm charge, to $\sim$185 μsec, 127-cm away from 0.2-gm charge at 10^{-5} Torr. Rise times were generally shorter at 10^{-3} and 10^{-4} Torr; the 10^{-5} Torr values agree with numerical calculations. Using cube root scaling of charge mass, the observed peak reflected pressure as a function of range may be represented by

$$p = 6.5 \times 10^5 \text{ (bar) } r'^{-3.5},$$

where r' the ratio of the range to the equivalent charge radius.

INTRODUCTION

Description of the expansion of the detonation products from a chemical explosion in vacuum is important to both developing appropriate gas equations of state as well as to the potential applications of explosives in vacuum environments. Theoretical and computational studies describing the phenomena associated with the detonation of explosives in vacuum were first carried out earlier by Thornhill[1] and Lutzky.[2] A number of authors[3-8] have described various aspects of the flows resulting from the free-expansion of a polytropic gas sphere into vacuum.

The available analytic descriptions of the free expansion of gas in either an initially uniform, or self-similar, density distribution in vacuum are appropriate for descriptions of the expansion clouds of gas which are initially at rest at a relatively low density. In practice such clouds might be produced as the result of the release of chemical propellant products in vacuum. In order to describe the expansion of solid or liquid high-explosive detonation products, the results discussed above can provide only approximate results since the sphere of gas produced from solid or liquid explosives differ significantly in two respects from static polytropic gas spheres.

First, because of the high initial densities of the detonation products ($\sim$2 g/cm^3), the gas cannot be described by single polytropic exponent equation of state as expansion into vacuum occurs. Experimentally, it is found that the polytropic exponent

$$k = -d \log v / d \log p$$

varies from $\sim$3 in the vicinity of the Chapman–Jouguet pressure to $\sim$1.3 to 1.5 at the distensions corresponding to $\sim$1 atmosphere.[9] Here p is pressure and v is specific volume. A second inadequacy of the static polytropic gas model for the detonation products, is that upon detonation of an explosive, the detonation wave imparts a particle velocity which is on the order of $\sim$2 km/sec to the gaseous and solid products. This velocity, at least initially,coincides with the direction of propagation of the detonation wave. Approximate analytic formulas describing the velocity of the leading edge of the flow of detonation products from a solid explosive in vacuo are available,[3] however, in practice complete solutions for the pressure, density, and particle velocity, and internal energy profiles as a function of time and space are obtained using numerical techniques. Numerical techniques are required largely because of the observed decrease in the effect of polytropic exponent of the detonation gas, k, as expansion from the Chapman–Jouguet state occurs.

Measurements of the speed of the ambient gas and gaseous products from detonating TNT and PETN have been carried out by Lundborg[10] in various vacuums down to 10^{-3} Torr. He observed apparent velocities in the range 9.2 to 19 km/sec. The 9.2 km/sec value was attributed as being characteristic of the explosive products while the higher observed speeds (e.g., 19 km/sec) were attributed to elastic collisions of the detonation gas with the initial distended atmosphere surrounding the charge. The present paper describes the first experimental measurements of gas flow speeds and pressure profiles at relatively large distances from the charge [(radius from charge/charge radius) approximately 400] in vacuums down to 10^{-5} Torr. Pressure profiles are measured as the detonation products strike a series of rigid surfaces placed at various radii from the charge. The speed of the leading front

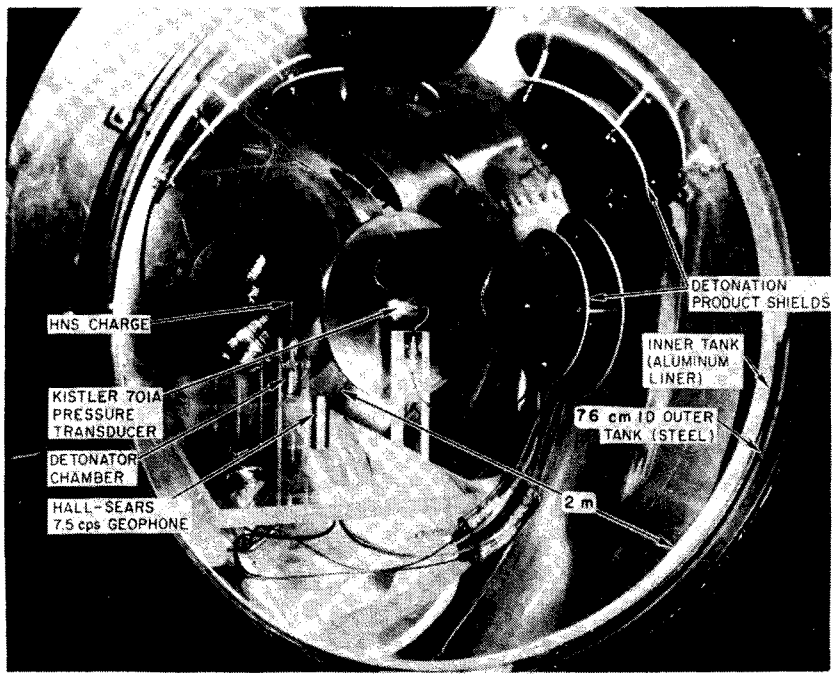

FIG 1. Experimental arrangement for measuring explosive gas blast in vaccum tank.

of the detonation gas, that is the speed of the explosive gas blast, is measured, and compared to approximate analytic solutions derived from the Landau and Stanyukovich[8] formulation for plane flow and using numerical results obtained by Mader[9] using the Becker–Kistiakowsky–Wilson equation of state. Numerical calculations of gas flows with real equations of state for the detonation products are used to obtain theoretical pressure and energy profiles. The pressure profiles are compared with the experimental data. The calculated energy profiles lead to an increased physical understanding of the observed phenomena.

GAS BLAST EXPERIMENTS IN VACUUM

A conventional (~830-liter) carbon steel vacuum tank was used to contain the experiments (Fig. 1). This tank was fitted with a removable aluminum liner upon which the carbon produced by detonated explosive charge was deposited. The liner was removed and carefully cleaned after each shot. A vacuum of 5×10^{-6} Torr was produced in the empty tank in 24 h by using a 6-in. NRC diffusion pump. In most of the experiments (see Table I) vacuums of 5×10^{-3} to 5×10^{-5} Torr were employed. The mean free path of O_2 or N_2 at these vacuums are on the order of several centimeters and $1\frac{1}{2}$ m, respectively. These pressure levels were chosen using the criterion that the mean free path of the molecules should be equal to, or greater than the tank dimensions. This criterion appears valid, since the experimental gas blast rise times measured at 5×10^{-5} Torr agree well with numerical calculations which assume ideal vacuum.

Pressed cylindrical pellets (diameter approximately equal to height) of pure HNS (hexanitrostilbene) and HNS/Teflon (90%/10%) were employed as the explosives in the experiments. These explosives were chosen because pure HNS is relatively easy to detonate in small quantities and HNS/Teflon is to be used as an explosive energy source in the course of the initial active seismic experiments on the moon. (High density TNT, for example, energetically almost equivalent to HNS, is much more difficult to detonate in small quantities.) The pure HNS pellets were detonated at one end using a mild detonating fuze (MDF). The end of the cylindrical charge which is detonated is confined by the stainless-steel tube, hence, the geometry of detonation in the pellet is similar to that which would take place in a hemisphere of explosive. The MDF, completely confined in stainless-steel tubing, is in turn detonated by an exploding bridgewire detonator. Fragments from the detonator are completely contained in a pipe. The HNS/Teflon pellets require a small booster (0.2 g of 1.6 g/cm³ pure HNS) in order to obtain reliable detonation.

Kistler Type 601A piezoelectric pressure transducers and modified Brüel and Kjaer (B&K) Type 4135 condenser microphones were used to detect the arrival time of the gas blast front at various distances from the charge, as well as to record the pressure (versus time) profile. This technique resembles that used for experiments at simulated high altitudes (minimum pressure, 0.7 Torr).[11] The pressure profile or "reflected shock pressure" was measured by mounting the pressure-sensitive element of the B&K microphone or Kistler transducer flush with the front surface, and in the center of, an aluminum plate with a diameter of 38 or 43 cm. [The response of one or more geophones (seismometers) (see Fig. 1) were also studied.[12]]

TABLE I. Gas blast arrival time and peak reflected pressures.

Shot No.	Environmental pressure (Torr)	HNS charge mass (g)	HNS charge density (g/cm³)	Distance (cm)	Distance in charge radii	Scale distance for 454g (1 lb) charge (m)	First arrival (μsec)	Rise time (μsec)	Amplitude (mV)	Gage No.[a]	Sensitivity (V/bar)	Peak reflected pressure (bar)
37–12297	5.5×10^{-5}	2.623	1.609	20.3			19±2	34±2	8500±100	K-2	1.79	4.75±0.06
38–12298	4.9×10^{-5}	2.620	1.606	20.3	28	1.13	21±1	28±2	8650±100	K-2	1.79	4.83±0.06
39–12299	4.4×10^{-5}	2.603	1.599	20.3			21±1	29±2	11 600±100	K-2	1.79	6.48±0.06
64–12446	3.9×10^{-6}	b	b	38.1	51	2.03	42±4	46±5	400±150	K-2	1.79	0.234±0.084
28–12269	5.0×10^{-5}	2.630	1.607	38.1			32±1	18±2	550±5	K-1	3.26	
32–12273	6.3×10^{-5}	2.647	1.615	38.1			32±2			K-1	3.26	
33–12274	5.6×10^{-5}	2.617	1.596	38.1	52	2.13	31±3	51±3	2660±50	K-1	3.26	0.816±0.016
34–12275	5.0×10^{-3}	2.618	1.597	38.1			38±2	10±2[e]	460±10	K-1	3.26	0.141±0.002
36–12296	6.4×10^{-6}	2.595	1.595	38.1			37±2	42±2	1150±10	K-2	1.79	0.642±0.006
64–12446	3.9×10^{-5}	b	b	50.8	68	2.61	47±2	48±5	1000±300	K-1	3.26	0.298±0.092
35–12295	6.2×10^{-5}	2.595	1.594	50.8			56±3	49±3	700±10	K-1	3.26	0.214±0.003
36–12296	6.4×10^{-5}	2.595	1.595	50.8	70	2.84	50±2	58±2	570±10	K-1	3.26	0.175±0.003
37–12297	5.5×10^{-5}	2.623	1.609	50.8			48±3	57±3	670±15	K-1	3.26	0.205±0.004
38–12298	4.9×10^{-5}	2.620	1.606	76.2	104	4.26	54±5[e]	41±5[e]	30±8[d]	K-1	3.26	0.0092±0.0028
39–12299	4.4×10^{-5}	2.603	1.599	76.2			54±4[e]	36±4[e]	25±2[d]	K-1	3.26	0.0077±0.0006
14–12255	5.8×10^{-6}	0.201[e]	1.60[f]	38.1			35±5	20±2	78±20	K-1	3.26	0.0239±0.0061
16–12257	2.6×10^{-5}	0.201[e]	1.60[f]	38.1			35±2	32±2	103±5	K-1	3.26	0.0316±0.0015
17–12258	3.3×10^{-6}	0.201[e]	1.60[f]	38.1			36±2	34±2	162±5	K-1	3.26	0.0497±0.0015
18–12259	5.0×10^{-3}	0.202	1.60[f]	38.1			46±2	15±2	315±20	K-1	3.26	0.0966±0.0091
22–12263	6.0×10^{-3}	0.202	1.60[f]	38.1			52±2[g]	28±2	550±20	K-1	3.26	0.1686±0.0061
23–12254	5.0×10^{-3}	0.202	1.60[f]	38.1			44±1	14±1	460±5	K-1	3.26	0.141±0.0015
62–12437[h]	3.8×10^{-6}	0.200	1.610	38.1	122	5.00	72±5[g]	42±5[g]	62±10	K-2	3.23	0.019±0.003
63–12445[h]	3.4×10^{-5}	0.1985	1.603	38.1			43±5	68±5	56±3	K-2	3.23	0.017±0.001
72–12522	4.5×10^{-5}	0.202	1.626	38.1			32±5	22±5	25±3	K-2	1.79	0.014±0.002
73–12523	4.6×10^{-5}	0.200	1.616	38.1			33±4	24±4	29±3	K-2	1.79	0.016±0.002
74–12524	4.4×10^{-5}	0.1985	1.610	38.1			33±2	22±2	21±1	K-2	1.79	0.012±0.001
75–12525	4.0×10^{-5}	0.2005	1.621	38.1			31±3	28±5	17±2	K-2	1.79	0.010±0.001
93–12651	4.2×10^{-5}	0.199	1.606	38.1			30±3	31±5	30±3	K-2	1.79	0.017±0.002
94–12652	4.4×10^{-5}	0.202	1.626	38.1			32±4	26±5	32±1	K-2	1.79	0.018±0.001

TABLE I. (*Continued*)

Shot No.	Environmental pressure (Torr)	HNS charge mass (g)	HNS charge density (g/cm³)	Distance (cm)	Distance in charge radii	Scale distance for 454g (1 lb) charge (m)	First arrival (μsec)	Rise time (μsec)	Amplitude (mV)	Gage No.[a]	Sensitivity (V/bar)	Peak reflected pressure (bar)
114–12726[i]	3.4×10^{-6}	2.612	1.600	101.6			129±20	140±20	12 500±100	M-2	+36 482 −118	+0.0087 0.0259 −0.0020
					139	5.67						
							127±10	145±20	12 200±100	M-2	+38 504 −123	+0.0081 0.0242 −0.0019
115–12727[i]	2.9×10^{-5}	2.610	1.601	101.6								
60–12435	2.7×10^{-5}	0.200	1.616	50.8			41±4	34±4	17.5±0.5	K-2	3.23	0.0054±0.0001
61–12436	3.5×10^{-5}	0.200	1.610	50.8					24±3	K-2	3.23	0.0074±0.0009
99–12657	3.5×10^{-5}	0.2017	1.653	50.8			54±5	66±5	4650±20	M-2	+79 545 −111	+0.0022 0.0085 −0.0011
					164	6.67						
100–12658	3.3×10^{-5}	0.2025	1.661	50.8			54±5	70±5	4450±30	M-2	+79 545 −111	+0.0021 0.0082 −0.0011
100–12658	3.3×10^{-5}	0.2025	1.661	50.8			46±3	24±2	5.8±0.2	K-2	1.79	0.0032±0.0001
58–12433	5.1×10^{-6}	0.201	1.639	63.5			51±15[g]	34±15[g]	6.2±1.0	K-2	3.23	0.0019±0.0003
59–12434	5.0×10^{-5}	0.202	1.616	63.5					6.4±0.5	K-2	3.23	0.0020±0.00015
					204	8.35			1900±200	M-2	+58 494 −110	+0.0017 0.0038 −0.0007
98–12656	2.4×10^{-6}	0.200	1.631	63.5								
101–12659	3.0×10^{-5}	0.2032	1.664	76.2			78±10	136±10	1250±50	M-2	+43 486 −114	+0.0009 0.0026 −0.0003
					245	10.00						
							84±10	111±10	1350±50	M-2	+43 486 −114	+0.0009 0.0028 −0.0003
102–12660	2.1×10^{-5}	0.2006	1.611	76.2								

103–1266[i]	2.4×10^{-5}	0.1994	1.613	101.6			126±2	133±5	470±10	M-2	+27 432 −108	+0.00039 0.00109 −0.00009
104–12716[i]	2.9×10^{-5}	0.1005	1.610	101.6			138±5	150±5	415±20	M-2	+300 476 −118	+0.00034 0.00087 −0.00009
105–12717[i]	4.4×10^{-5}	0.1997	1.590	101.6			134±3	171±3	466±5	M-2	+31 495 −125	+0.00033 0.00094 −0.00006
108–12720[i]	1.5×10^{-4}	0.2008	1.611	101.6	327	13.32	130±5	200±20	490±15	M-2	+24 491 −123	+0.00037 0.00100 −0.00008
109–12721[i]	1.1×10^{-4}	0.2008	1.616	101.6			128±5	194±50	460±10	M-2	+23 466 −116	+0.00035 0.00099 −0.00007
110–12722[b,i]	4.8×10^{-5}	0.200	1.625	101.6			145±20			M-2	+23 483 −121	
106–12718[i]	6.2×10^{-5}	0.1998	1.603	127.0			144±10	180±20	190±10	M-2	+22 459 −116	+0.00017 0.00041 −0.00004
107–12719[i]	3.5×10^{-5}	0.200	1.606	127.0	409	16.65	138±10	190±20	175±20	M-2	+23 489 −124	+0.00017 0.00036 −0.00006

[a] K-1 and K-2 Kistler Type 701A pressure transducers. M-2 modified Brüel and Kjaer microphone.
[b] HNS/Teflon (90%/10%); mass = 2.785 g, ρ = 1.73 g/cm³. HNS booster; mass = 0.200 g, ρ = 1.637 g/cm³.
[c] Onset of sharp increase in pressure, possibly not first arrival.
[d] Results possibly disturbed as a result of disturbance from chamber wall.
[e] Nominal charge mass ±0.001 g.
[f] Nominal charge density ±0.010 g/cm³.
[g] Onset of pulse uncertain.
[h] Shot inclined 45° toward transducer.
[i] Metal protective grid on microphone replaced with nylon grid.

TABLE II. Characteristics of explosive gas blast from HNS in vacuum.

Nominal charge mass (g)	Distance (cm)	Vacuum (Torr)	Gas blast velocity (km/sec)		Rise time of gas blast (μsec)		Reflected shock pressure (bar)	
			Measured	Flow calculations[a]	Measured	Flow calculations	Measured	Flow calculations
0.201	38.1	5×10^{-3}	8.0	...	19	...	0.14±0.03	
0.201	38.1	5×10^{-5}	12.0	8.97[b]	37+10	57[b]	0.021±0.008	0.063[b]
					−7	61[c]		0.056[c]
						40[d]		0.031[d]
				7.75[c]				
				6.80[d]				
2.60	38.1	5×10^{-3}	10.8[e]	...	14	...	0.14	
2.60	20.3	5×10^{-5}	10.3	...	30	...	5.4±0.6	
2.60	38.1	5×10^{-5}	11.4	6.93[d]	47	40[d]	0.73±0.09	
2.60	50.8	3×10^{-5}	9.90	6.77[d]	55	55[b]	0.20±0.02	
0.201	101.6	3×10^{-5}	7.6[e]	8.97[b]	170±30	142[b]	0.0010±0.0001	0.0033[b]
						159[c]		0.0031[c]
				7.75[c]				

[a] For plane flow the leading edge of the gas blast, depending on the assumed equation of state, has a calculated velocity of 10.2 to 13.0 km/sec.
[b] LSZK equation of state variable cell thickness (D. Gerneth, private communication).
[c] Wilkins equation of state, uniform cell thickness $U_0=0.098$ Mbar cm³/cm³.
[d] Wilkins equation of state, uniform cell thickness $U_0=0.060$ Mbar cm³/cm³.
[e] Less certain data.

The Kistler transducers and B&K microphones were used in the overlapping pressure ranges of 10^{-3} to 10 bar and 10^{-6} to 10^{-2} bar, respectively. The Kistler transducers are believed to be less reliable than the microphones in the range from 10^{-3} to 10^{-2} bar. The outputs of the Kistler transducers were preamplified using Endevco Type 2616.1B charge amplifiers placed immediately outside the vacuum tank. Calibration of the Kistler transducers is described in Appendix A.

The B&K microphones, when operated in air, rely on the viscous drag of air flowing in and out of a small cavity behind the pressure-sensing diaphragm for damping. In hard vacuum, serious oscillation of the diaphragm occurs unless damping is introduced by other means. We placed a small plug of polyurethane foam between the diaphragm and a specially made slotted nylon grating in front of the microphone to obtain damping. The grating, which replaces the standard metal screen, permits calibration of the damped microphone in vacuum with an electrostatic actuating device (see Appendix B). A Type 2615 B&K cathode follower, was placed in the vacuum tank with the microphone. The standard B&K Type 2801 power supply and output impedance control unit was placed immediately outside the vacuum.

Calibration tests of the modified B&K microphone (Appendix B) indicated that the absolute microphone sensitivity in vacuum increased (by a factor of 3 to 8) over that in air as the frequency increased from 10 to 25 kHz.

In the analysis of the microphone recordings the signal period was estimated by assuming it to be equal to four times the observed pressure-pulse rise time. A check on the adequacy of this procedure for obtaining appropriate calibration factors was made by taking the Fourier integral of one of the microphone records and convolving the spectrum with the measured amplitude response (assuming a zero phase shift at all frequencies). Upon casting the convolved voltage signal back into the time domain the amplitude of the resulting pulse can be compared with the amplitude obtained by estimating the predominant frequency component from the rise time (Fig. 3). In general, the reconstructed pressure pulse had a lower high-frequency content than the original pulse and the front of the pulse is ill-defined because of the lack of phase information. However, the value of the peak pressure is not strongly affected by the phase uncertainty. For example, the amplitude obtained from the frequency analysis for shot 99–12657 is 0.0078 bar which compares favorably with that obtained from the simple analysis (0.0085+0.002, −0.0011 bar).

EXPERIMENTAL RESULTS

In most of the experiments, cylindrical pellets (diameter approximately equal to height) were initiated with the axis of the MDF detonator assembly oriented at 90° to the direction to the transducer. In order to establish whether the azimuthal symmetry of resulting detonation gas flow is strongly affected by detonating the cylindrical charge at one end (rather than in the middle of a spherical charge, as is assumed in the analytic solutions and computer calculations), shots were fired with the MDF-detonator assembly axis at 45° to and parallel to the direction to the pressure transducers. At 45° the pressure profile (shots 62–12437 and 63–12445) was similar to that observed at 90°. In one experiment in the parallel configuration (MDF-

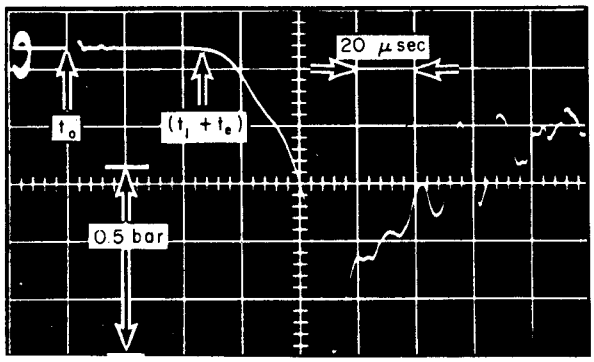

FIG. 2. Kistler pressure transducer record of explosive gas blast. (shot 33–12274, oscilloscope 3). Time increases from left to right. Increasing pressure is downward. Detonator pulse shown at time t_0. Gas blast arrives at t_0. Gas blast arrives at transducer at time (t_1+t_e). Time through explosive train (detonator and MDF), t_e, is measured in separate experiment. The 50-kHz ringing observed at the end of the record is believed to be caused by mechanical resonance of the transducer.

detonator assembly pointed at the transducer), an extremely large signal was recorded by the transducer and the surface facing the charge was blackened and pitted, presumably by the PETN detonator products and the molten lead from the MDF.

A unique feature of explosive gas blast in vacuum is the long rise time which is observed compared to that which would be associated with the corresponding shock wave in air. The observed rise time is dependent on ambient pressure and propagation distance (Table II). The long rise time of gas blast as it interacts with an incompressible boundary can be seen in Figs. 2 and 3 (e.g., ~50 and ~150 μsec at 38 and 102 cm from a 0.2-g charge). (The rise time of the Kistler transducers is given by the manufacturer as 3 μsec. Calibration of the modified B&K microphone indicates that the rise time of this instrument is about 2 μsec.) After the peak

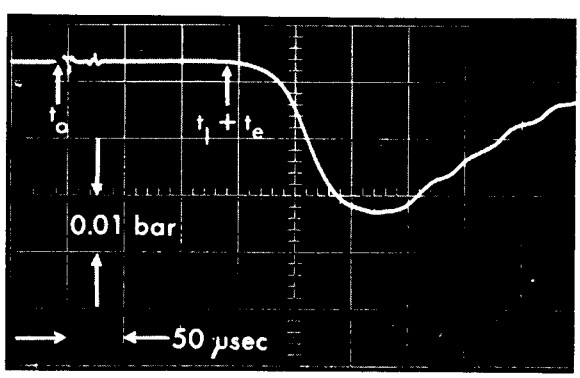

FIG. 3. Modified B&K microphone record of explosive gas blast (shot 114–12726). Time increase from left to right. Increasing pressure is downward. Detonator pulse shown at time t_0. Gas blast arrives at microphone at time (t_1+t_e).

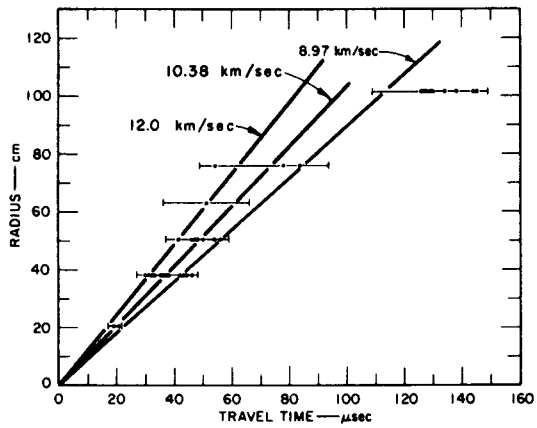

FIG. 4. Radius of transducer of microphone from center of charge versus gas blast arrival time. Velocities of leading edge of gas blast from various calculations are indicated.

pressure is achieved, the pressure decays, even in the idealized case of spherical flow impinging on a spherical concentric boundary. Although the incompressible (flat) surfaces used are finite in extent, the pressure in the center of the plate is not affected by flow around the plate edges for a time interval which corresponds to the acoustic-wave travel time in the stagnated detonation products. For example, for a 200-bar stagnation pressure and a 38-cm-diam plate the time required for the first disturbance to arrive at the transducer position at the center of the plate is ~230 μsec. For lower stagnation pressure (all less than 7 bar in the present experiments) the time interval corresponding to the arrival of rarefaction waves at the transducer from the plate edge is substantially greater.

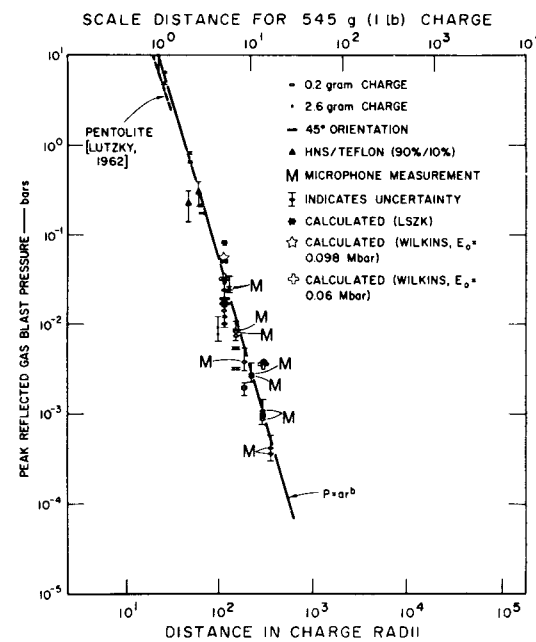

FIG. 5. Reflected gas blast pressure versus distance in charge radii.

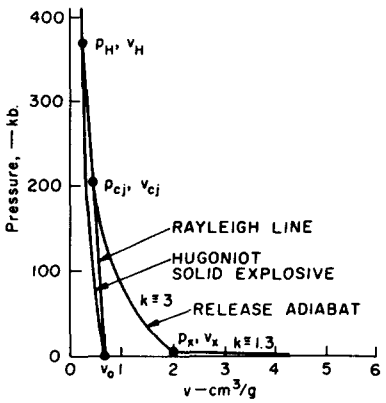

FIG. 6. Pressure–volume plane. p_H, v_H is Hugoniot state in undetonated explosive; p_x, v_x is transition state at which polytropic exponent of detonation gas adiabat changes from $k\cong 3$ to $k\cong 1.3$. Rayleigh line has slope of $-(D/v_0)^2$.

The gas-blast rise times (Table I and II) observed at ambient pressures of 5×10^{-5} Torr are in general agreement with the rise times obtained in a corresponding computer calculation. This agreement indicates that for present experimental purposes the gas blast characteristics as measured at the 5×10^{-5} Torr vacuum level are effectively those existing in an ideal vacuum. (The rise times observed under 5×10^{-3} Torr are appreciably shorter than under 5×10^{-5} Torr.)

Another striking feature of the explosive gas-blast phenomenon is the high speed with which the leading edge of the gas blast travels outward from the detonated charge (Fig. 4). Of specific interest in Table II are the slightly lower velocities obtained with the 0.2-g charges at 5×10^{-3} Torr compared with those obtained at 5×10^{-5} Torr. This is probably the results of the residual gases in the vacuum chamber interacting with the outward-flowing detonation products. As can be seen in Table II, the observed gas blast velocities range from 8 to 12 km/sec; these velocities are somewhat higher than, but still of the same magnitude as, those predicted by the computer calculations. The approximate analytic formulas and calculations, based on the actual equation-of-state for HNS, predict values of u_f ranging from 10.2 to 13.0 km/sec.

To relate pressure profiles observed in small-scale vacuum experiments to those which would be produced with large charges at distances far greater than those attainable even with the largest of vacuum chambers, it is important to be able to scale experimental and calculational results.

Following Stanyukovich we have used the charge mass and, hence, the radius of an equivalent sphere of explosive as the scaling parameter to compare experiments employing different charge masses with each other and with the computer calculations.

Except for shots fired at pressures of 5×10^{-3} Torr, for which the pressure profiles recorded were probably affected by residual gases in the vacuum tank, the reflected pressure data at different distances, using various charge masses, lie along a single curve constructed with cube root scaling (Fig. 5). Furthermore, since the data and the results of the calculations (see next section) appear to lie along a straight line in the log (maximum) pressure–log radius ratio plane, the usual power law for the maximum reflected shock pressure from charges is suggested:

$$p=ar'^b. \tag{1}$$

For the data shown in Fig. 5, we find that $a=6.5\times10^5$ bar and $b=-3.5$. Here p is reflected shock pressure in bars and r' is the ratio of distance from the charge center to the radius of the charge. This result differs significantly from that discussed by Fletcher *et al.*[13] for the expansion of certain propellant products, (approximated by a sphere of ideal gas initially at rest, expanding in a vacuum); these investigators found that $b=-3$. We note further that the value of b is in close agreement to that inferred from the higher-pressure calculations of Lutzky in which the pressure profile from a 454-g pentolite sphere detonated in vacuum was obtained. The value of b also agrees well with calculations performed using either a Landau–Stanyukovich–Zeldovich–Kompaneets[2] (LSZK) or a Wilkins equation of state for TNT and similar boundary conditions. The values of the reflected shock pressures for HNS lie between the calculated values for pentolite and TNT. In general, measured values might be expected to lie below calculated ones, especially at smaller radii, since the experimental obstacle, a plate (38 or 43 cm in diameter), is flat and thus an approximation to the concentric spherical shell assumed in the calculations.

CALCULATING GAS BLAST VELOCITY

The velocity achieved by the leading edge of the detonation products as these expand adiabatically outward in vacuum for the one-dimensional planar flow may be calculated. Knowledge of the detonation, or Chapman–Jouguet, state and the reacted, or adiabat curve of the detonation products centered at the Chapman–Jouguet pressure–volume–energy (p_{cj}, v_{cj}, u_{cj}) state is required (Fig. 6). The particle velocity, u, of a mass element upon isentropic expansion is given by

$$u=u_{cj}+\int_{v_{cj}}^{v}\frac{c\,dv}{v}, \tag{2}$$

where u_{cj} indicates the Chapman–Jouguet state, and c and v are the sound velocity, and specific volume along the isentrope.

At pressures between the Chapman–Jouguet state ($P_{cj}\cong200$ kbar and $v_{cj}\cong0.6$ cm³/gm) and an intermediate state ($p_x\cong3$ kbar, $v_x\cong2$ cm³/gm), the isentrope of the product gas can be approximated by a polytropic equation of state (where $k=n\cong3$).[14] At lower pressures the polytropic exponent is close to 1.3 or 1.4. The sound speed at a point along the isentrope is

$$dv/v=[-2/(k-1)](dc/c). \tag{3}$$

Approximating the isentrope by two polytropes with $k=n$ above p_x and $k=\gamma$ below p_x and substituting Eq. (13) into Eq. (2) gives[14]

$$u_f=u_{cj}-\frac{2}{n-1}\int_{c_{cj}}^{c_x}dc-\frac{2}{\gamma-1}\int_{c_{x'}}^{0}dc. \tag{4}$$

The polytropic exponent changes discontinuously at p_x, v_x, the two values c_x and c_x' are defined by

$$[(dp/d\rho)_s]^{1/2}=c_x^+ \tag{5a}$$

and

$$[(dp/d\rho)_s]^{1/2}=c_x^-, \tag{5b}$$

The upper limit of the second integral in (4) is zero since the sound speed upon infinite expansion goes to zero. When $n\cong 3$, the gas sound speed plus the particle velocity at the Chapman–Jouguet state equals the shock (or detonation) velocity in the unreacted explosive D, Eq. (4) is then

$$u_f=D+c_x+[2/(\gamma-1)]c_x'. \tag{6}$$

Here $c_x=(np_xv_x)^{1/2}$ and $c_x'=(\gamma p_xv_x)^{1/2}$. To estimate the p_x, v_x, state, we note that the total internal energy at the Chapman–Jouguet state U_{cj}, is

$$U_{cj}=\frac{p_{cj}v_{cj}}{n-1}-\frac{p_xv_x}{n-1}+\frac{p_xv_x}{\gamma-1}+\frac{pv}{\gamma-1}. \tag{7}$$

Since the temperature at p_x, $v_x(p_xv_x/R)$ is much greater than at p, v it follows that $p_xv_x\gg pv$ so the last term in (7) may be neglected. Also,

$$U_{cj}\cong Q+\tfrac{1}{2}p_h(v_0-v_h), \tag{8}$$

where Q is the heat of detonation and the second term comes from the shock energy conservation relation. From the Rankine–Hugoniot relations,

$$D^2/v_0^2=p_h/(v_0-v_h), \tag{9}$$

Recognizing that the Chapman–Jouguet state also lies along the Rayleigh line,

$$p_h/(v_0-v_h)=p_{cj}/(v_0-v_{cj}). \tag{10}$$

Equation (9) represents the negative slope of the isentrope passing through the Chapman–Jouguet state or

$$(dp/dv)_{p=p_{cj}}=-p_{cj}/(v_0-v_{cj})=-p_h/(v_0-v_h), \tag{11}$$

since the isentrope passing through the Chapman–Jouguet state is given by $pv^n=\text{constant}$

$$D^2/v_0^2=np_{cj}/v_{cj}. \tag{12}$$

From Eqs. (9), (11), (12), it also follows that

$$(v_{cj}/v_0)^2=[n/(n+1)]^2, \tag{13}$$

and solving Eq. (8) for p_xv_x yields

$$p_xv_x=\frac{\{Q-D^2/[2(n^2-1)]\}(n-1)(\gamma-1)}{n-\gamma}. \tag{14}$$

Upon substituting Eq. (14) into (6) we get for the velocity of the leading edge of the detonation products

$$u_f=D+\left(n^{1/2}+\frac{2}{\gamma-1}\gamma^{1/2}\right)\times\left(\frac{\{Q-D^2/[2(n^2-1)]\}(n-1)(\gamma-1)}{n-\gamma}\right)^{1/2}. \tag{15}$$

In the case of HNS, Mader[15] has calculated a detonation velocity D, of 6.74 km/sec. Using 1 kcal/gm for Q, $n=3$, and $\gamma=1.3$, an escape velocity, u_f of 13.06 km/sec is obtained. If values of γ of 1.4 and 1.5 are assumed the u_f resulting are 12.90 and 12.91 km/sec. As can be seen in Fig. 4 these calculated values are somewhat high but of comparable magnitude as compared to the observed data. A somewhat simpler formula than Eq. (15) is derived by Zeldovich and Kompaneets who neglect the second and last term on the right-hand side of Eq. (7). In this case

$$p_xv_x\cong\left(Q-\frac{D^2}{2(n^2-1)}\right)(\gamma-1). \tag{16}$$

If following Zeldovich and Kompaneets, the discontinuous change of slope with the adiabat at p_x, v_x is neglected by only taking the value of c_x' at this point, Eq. (6) may be rewritten as

$$u_f=D+c_x'\left(\frac{\gamma+1}{\gamma-1}\right)=D+\left(\frac{\gamma+1}{\gamma-1}\right)\left[\gamma(\gamma-1)\left(Q-\frac{D^2}{2(n^2-1)}\right)\right]^{1/2}. \tag{17}$$

Using the same parameters as before Eq. (17) gives $u_f=10.85$ and 10.21 km/sec for values of u_f when γ is 1.3 and 1.4 respectively. This formula gives better agreement with the data.

It should be noted that the velocity achieved by the leading edge of a sphere of polytropic gas, initially at *rest* is also given by Eqs. (4) and (6). In this case $u_{cj}=0$, and v_{cj} and c_0 represent the initial specific volume and sound speed. The terminal velocity in the case of the "two polytropic" gas law adiabat

$$u_f=\frac{-2}{n-1}\int_{c0}^{c_x}dc-\frac{2}{\gamma-1}\int_{c_{x'}}^{0}dc, \tag{18}$$

where c_x and c_x' have the same meaning as before. If the polytropic exponent is a constant, equal to q, the final velocity is then

$$u_f=[2/(q-1)]c_0 \tag{19}$$

Still another way of estimating terminal speed of the leading edge of a volume of detonation gas expanding into vacuum is to extrapolate numerical calculations of the isentrope (which generally extend from the Chapman–Jouguet pressure to ~100 bar) to zero pressure. Mader[15] has performed a numerical calculation

TABLE III. Calculated escape velocity for polytropic gas initially at rest.

Escape velocity (u_f/c_0)		
$k=5/3$	$k=7/5$	Comments
3.00	5.00	Theoretical value
3.03	4.63	Planar flow, geometric series net
2.85	4.29	Spherical flow, geometric series net
3.12	4.90	Planar flow, uniform, and arithmetic series combination net
3.02	4.67	Spherical flow, uniform, and arithmetic series combination net

of the release adiabat passing through the Chapman–Jouguet state in HNS using a Becker–Kistiakowsky–Wilson equation of state. At the Chapman–Jouguet state of HNS with a loading density of 1.60 g/cm³, and a detonation velocity of 6.74 km/sec[2], $p_{cj}=192$ kbar, and $v_{cj}=0.460$ cm³/g, the effective polytropic exponent is 2.79. Upon isentropic expansion of the detonation products to 107 bar and a volume of 24.9 cm³/g the effective polytropic exponent is 1.50 and the intermediate particle velocity u_i is 8.1 km/sec. The intermediate sound speed at the 107-bar state is 0.634 km/sec. Extrapolating Mader's results to infinite expansion, and hence zero pressure, using the formula

$$u_f=u_i+[2/(k-1)]c_i \qquad (20)$$

gives a velocity of 10.62 km/sec which is in good agreement with the experiments and the approximate calculations discussed above.

It follows from Eqs. (15) and (17) that for rarefaction from steady state the speed achieved by the leading edge of the detonation product gas upon free expansion in vacuum depends on the Chapman–Jouguet state and equation of state of the gas. This speed is independent of geometry. It should, however, be emphasized that pressure and particle velocity profiles do depend on geometry.

COMPLETE FLOW CALCULATIONS

A series of calculations was performed in which the detonation of spherical charges of TNT (chemically similar to HNS), the expansion of the detonation gases into a perfect vacuum, and the interaction of these gases with a spherical incompressible boundary were numerically described. The initial sphere of explosive is subdivided into a number of constant mass spherical shells or cells. The computation scheme employed is similar to that presented by Herrmann *et al.*[16]

Initial calculations carried out with constant thickness cells yielded reasonably shaped reflected pressure profiles but gave too low a velocity for the expanding gas front, e.g., 7 km/sec versus the 8 to 12 km/sec observed.

In order to develop an adequate computational procedure so as to give the correct velocity of the leading edge of the gas front, a series of numerical experiments was performed assuming a uniform sphere of gas and using a polytropic equation of state. The cell thicknesses were either taken as constant or made a decreasing function of radius according to either a geometric or an arithmetic progression. Calculations were run using between 50 and 900 cells for $k=\frac{5}{3}$ and $k=\frac{7}{5}$ using uniform, arithmetic, and geometric spacing, as well as a combination of these. The outer cell thicknesses had to be on the order of 10^{-7} mm to achieve the theoretical gas front velocities. For this reason a combination arithmetic (near the free surface) and uniform net was employed in later calculations. It was found in the early runs that the difference equations were unstable when particle speeds neared the theoretical value of u_f. This instability was eliminated by introducing a limitation on the time step, so that changes in a variable could not propagate faster than the particle speed, when particle speeds exceeded the sound or shock speed. This limitation is in addition to the conventional one that limits the time step so that changes in the variable cannot propagate faster than the sound or shock speed. The time step change is also limited to a 10% difference from that used in the previous time step. The calculations for the gas front speed in planar flow agree with the theoretical results within a few percent (see Table III). The results also indicate that the speed of the leading gas front is the same in spherical flow as in planar flow. Using the variable cell spacing, we found that the leading edge of the gas, from either a plate or a sphere (planar or spherical symmetry) initially at rest, achieved the theoretical velocity, $u_f=2c_h'/(\gamma-1)$. In this way, using variable net spacing, the cell thickness in a 0.5-mm radius sphere of explosive will vary from 10^{-1} mm near

TABLE IV. Equation of state parameters, TNT.[a]

p-v-U Relations [Eqs. (3) and (4)]	Burn fraction calculation
$A=3.7377$ mbar	U_0 (detonation energy) $=0.06$ mbar cm³/cm³
$B=0.03747$ mbar	ρ_0 (initial density) $=1.63$ g/cm³
$C=0.0073383$ mbar	p_{cj} (detonation pressure) $=0.210$ mbar
$R_1=4.15$	D (detonation velocity) $=0.693$ cm/μsec
$R_2=0.9$	$k_{cj}=2.914$
$W=0.35$	

[a] M. Wilkins (private communication).

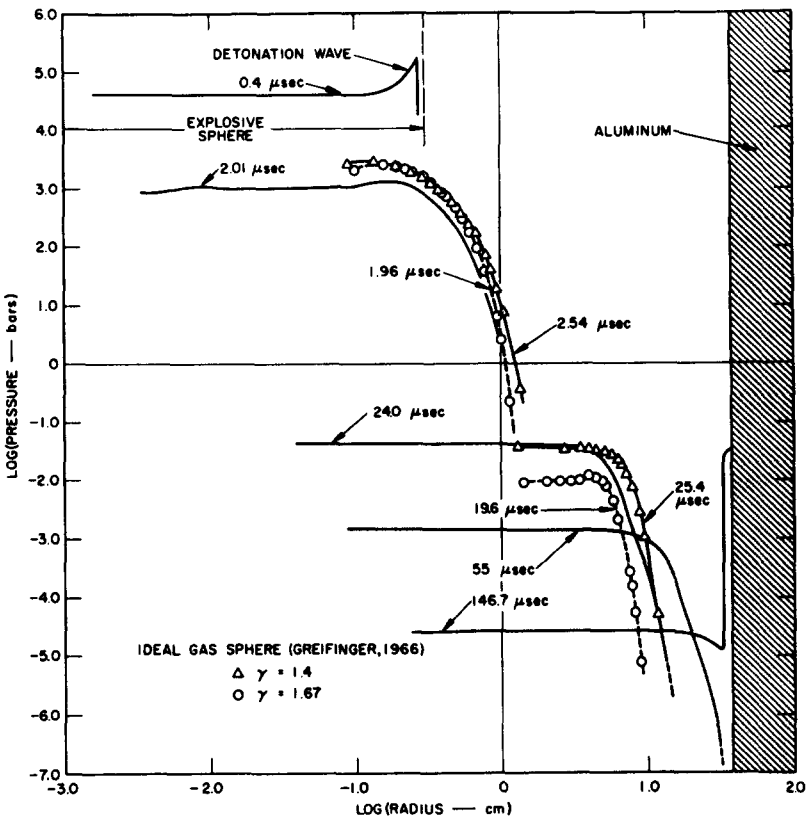

FIG. 7. Results of computer calculation, logarithm (to base 10) of pressure versus logarithm (to base 10) of radius at different times for 0.201-g TNT charge detonated in vacuum inside aluminum shell with radius of 38.1 cm. Wilkins equation of state with $E_0=0.060$ Mbar cm³/cm³ and 200 uniform thickness spherical cells was employed in calculations. Expansion of uniform sphere of ideal gas (calculated by Greifinger[18]) is shown for comparison.

the center of the explosive to 10^{-7} mm near the free surface.

In the initial calculations (200 uniformly spaced cells), the detonation of the explosive was described by the "burn fraction" method of Wilkins.[17] For the detonation gas, a Wilkins equation of state for TNT was used to represent the equation of state of HNS. (The chemical structures of HNS and TNT are quite similar.) The equation of state of TNT was

$$p=A(1-W/R_1V)\exp(-R_1V)+B(1-W/R_2V)\times\exp(-R_2V)+(WU/V). \quad (21)$$

In the pressure–volume plane, the adiabat is given by

$$p=A\exp(-R_1V)+B\exp(-R_2V)+C/V^{W+1}. \quad (22)$$

Here p is in megabars, V is relative compression $\rho'=\rho/\rho_0$, and U is energy (10^{12} erg) per cubic centimeter of the undetonated explosive. Numerical constants are listed in Table IV. The resulting pressure profiles for the detonation of a 0.402-g charge of TNT and the interaction with a spherical shell placed at 38.1-cm radius is shown in Fig. 7. The classic detonation wave profile is seen in the explosive at 0.4 μsec, just before the detonation wave breaks out into the vacuum. After this occurs, a marked and continuous drop in pressure takes place as the gas expands into the vacuum. A terminal gas front velocity of 6.8 km/sec is obtained in this calculation. A later set of calculations using the LSZK equation of state with uniform cells over the interior nine-tenths of the radius and cell dimensions defined by a decreasing geometric series over the outer one-tenth of the radius gave terminal velocities closer to those measured (Table II).

Greifinger[18] has calculated the free expansion of a sphere of ideal gas into a vacuum. For comparison, his results are shown in Fig. 7 at two times for which the two sets of calculations overlap. In Greifinger's calculations, performed at logarithmic time intervals, only a constant value of k was considered. Greifinger's units of time are $(k^{1/2}r_0/c_h')$, and have been appropriately scaled so that the radius of the initial sphere of gas corresponds to that of the solid explosive, 0.3084 cm. The detonation energy of 0.0368 Mbar cm³/g is simultaneously and uniformly released in the gas as kinetic energy so that the initial density of the ideal gas sphere is the same as that of the solid explosive, 1.63 g/cm³. The two sets of calculations show surprisingly good agreement considering the totally different assumptions in regard to the pertinent physical processes as well as in the assumed equation of state of the gases.

The physical processes involved in the expansion of

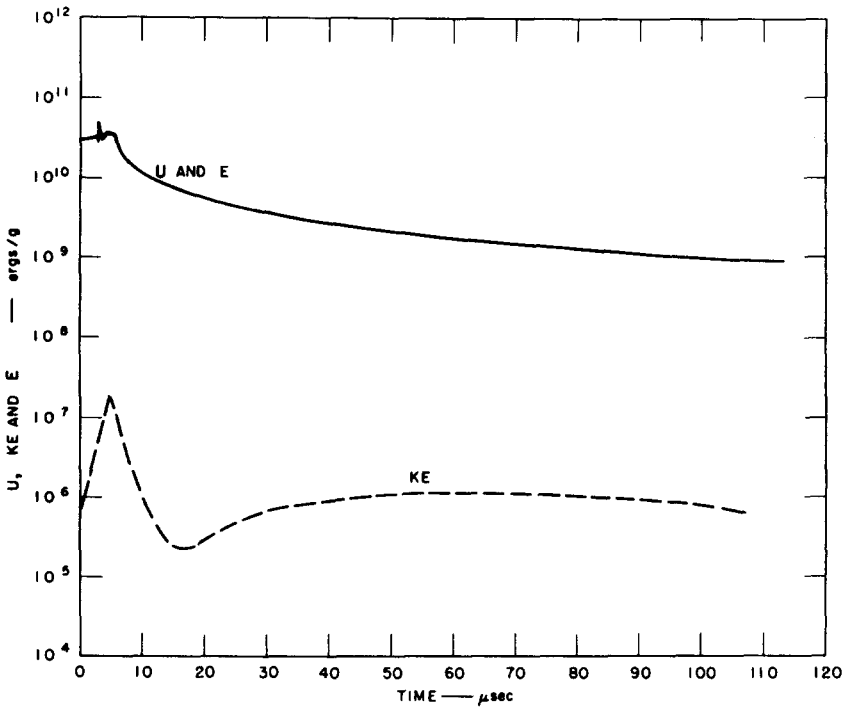

FIG. 8. Internal energy (U), kinetic energy (KE), and total energy E=U+KE for cell 1 (center of TNT charge) versus time. The curve for U and E are virtually identical. Because of low value relatively large numerical error is associated with the KE curve.

detonation gases in a vacuum can be illustrated by considering the changes in partition of energy within and between cells. These changes are shown in Figs. 8–10. Here the kinetic energy (KE), internal energy (U), and total energy (E) of several cells within the initial TNT sphere are plotted as a function of time. For cell 1 (the center cell) the kinetic energy remains at a nearly constant and relatively low value of $\sim 10^6$ erg/g. However, the internal energy and hence also the total energy are dramatically reduced beginning at ~ 5 μsec. This time corresponds to the arrival at the center of the explosive sphere of the rarefaction origi-

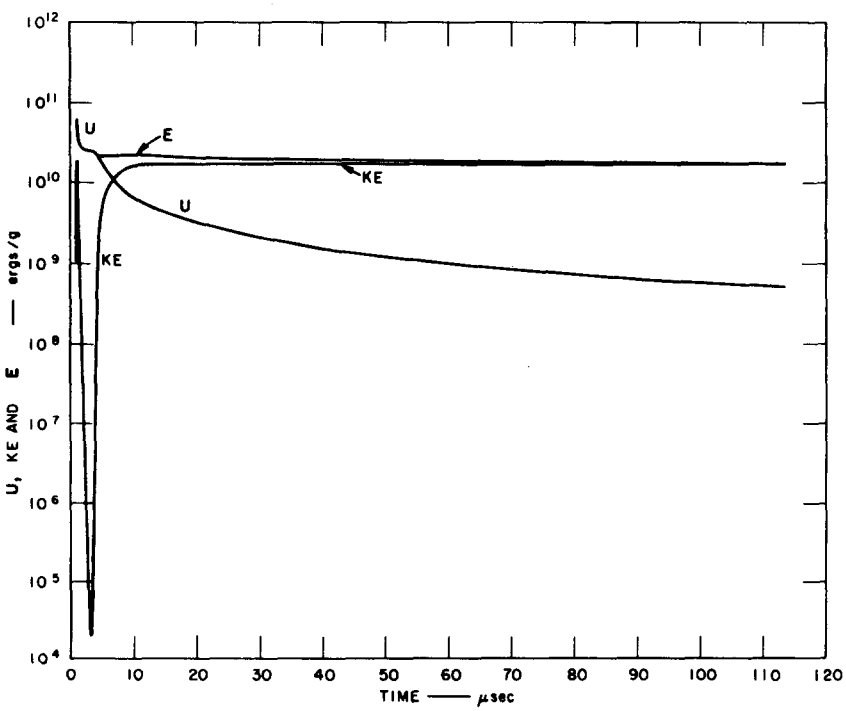

FIG. 9. Internal energy (U), kinetic energy (KE), and total energy (E) for cell 100 (halfway along radius of TNT charge) versus time.

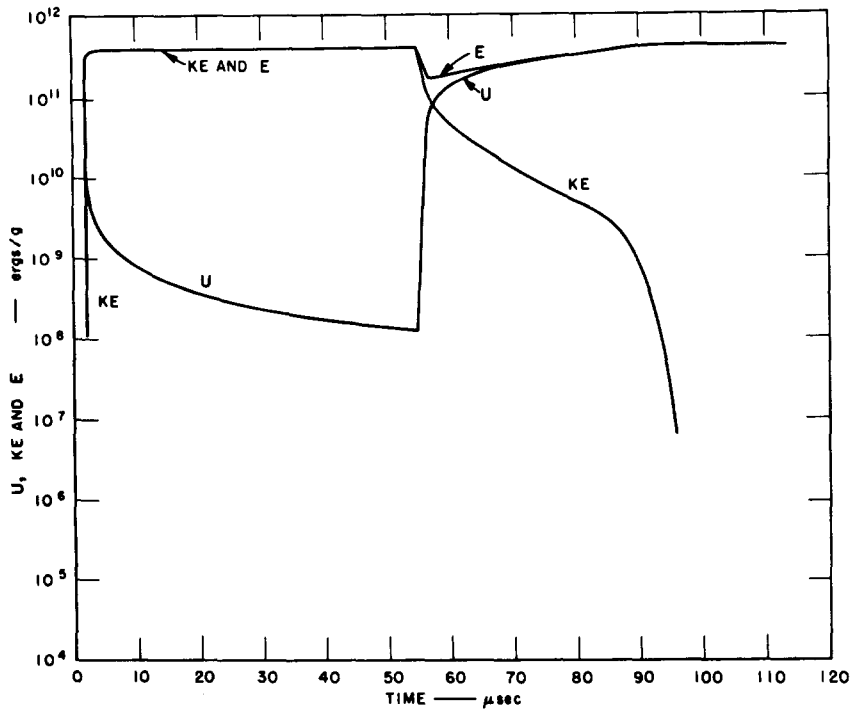

FIG. 10. Internal energy (U), kinetic energy (KE), and total energy (E) for cell 200 (outermost spherical shell of TNT charge) versus time.

nating at the explosive–vacuum interface. From the standpoint of symmetry, it can be concluded that a net outflow of energy takes place from the interior of the detonation gas sphere. In cell 100, halfway along the radius of the sphere, the internal energy and hence also the total energy behave in a similar manner to that in cell 1. The first maximum in kinetic energy probably is due to the passage of the detonation wave. Later (~3 μsec) the kinetic energy increases dramatically when the rarefaction wave arrives from the explosive-vacuum interface. As in cell 1, a net loss of energy with time is observed. In cell 200 (Fig. 10) (the outermost cell) the detonation wave is reflected at the free surface, and the internal energy decreases very rapidly from the value associated with the detonation state. This is accompanied by a rapid increase in both the total energy and kinetic energy. The interaction of the outer cell of gas with an incompressible spherical shell occurs at ~55 μsec. After this time the kinetic energy of cell 200 is sharply reduced and the internal energy increases as the reflected shock is driven back into the outward-flowing detonation gas.

Two features of the explosive gas blast phenomena brought out by Figs. 8–10 are as follows:

(1) The high terminal velocity (~10 km/sec) of the outermost detonation gases is achieved within a few microseconds (3–5) after the arrival of the detonation wave at the explosive free surface.

(2) A net outward flux of the specific energy per unit mass occurs within the expanding gas sphere with increasing time. The outer gas layers gain kinetic energy at the expense of their internal energy and at the expense of the total energy within the interior of the sphere.

SUMMARY AND CONCLUSIONS

Upon detonation of small (0.2- and 2-g) charges of HNS explosive in vacuums of 10^{-3} to $\sim 5\times10^{-5}$ Torr the resultant product gas blast rapidly achieves a terminal velocity of ~10 to ~12 km/sec. By measuring the resulting pressures at a series of plates placed at various radii from the charges the rise time to maximum stagnation ("reflected shock") pressure is observed to vary from ~30 μsec, at a radius of 20 cm from a 2.6-gm charge, to ~185 μsec, 127 cm from 0.2-gm charge. The gas blast rise times were generally shorter at 10^{-3} and 10^{-4} Torr than at $\sim 5\times10^{-5}$ Torr. Measured rise times at 5×10^{-5} Torr generally agree with accompanying numerical calculations.

The reflected peak pressure data may be represented by

$$p = 6.5\times10^{5}\ (\text{bar})\, r'^{-3.5},$$

where r', is the ratio of the radius from the center of the charge to the transducer to the radius of an equivalent spherical charge. The present data extends from 28 to 409 charge radii. The exponent of r' agrees with that obtained by Lutzky for the fall off of the gas blast at a distance of ~10 charge radii from a 1-lb PETN sphere detonated in vacuum.

The terminal velocity of the leading edge of ex-

panding detonation products may be calculated analytically by assuming that the release adiabat centered at the Chapman–Jouguet state of the detonation products can be approximated by two polytropic equations of state. Assuming $pv^k = \text{constant}$, taking the value $k = n \cong 3$ above some pressure p_x (~ 2 kbar) and a value of $k = \gamma \cong 1.3$ below p_x, and using the Chapman–Jouguet detonation theory, the terminal velocity at the leading edge of the detonation products is given by

$$u_f = D + \left(n^{1/2} + \frac{2}{\gamma - 1} \gamma^{1/2} \right) \times \left[\frac{[Q - D^2/2(n^2-1)](n-1)(\gamma-1)}{n-\gamma} \right]^{1/2}.$$

Here D and Q are the detonation velocity and heat of detonation of the explosive. For HNS, taking $D = 6.74$ km/sec, $Q = 1$ kcal/gm, $n = 3$ and $\gamma = 1.3$ a value of u_f of 13.1 km/sec is obtained. Extrapolating Mader's calculated Becker–Kistiakowsky–Wilson (BKW) adiabat for HNS to zero pressure yields $u_f = 10.6$ km/sec. The value u_f obtained from this latter calculation fit the experimental results.

Finite difference computations describing the outward flow of detonation products from an explosive (HNS or TNT) sphere in vacuum, and their interaction with an incompressible boundary show that the high terminal velocity of the outermost detonation gasses is achieved within 3 to 5 μsec after the arrival of the detonation wave at the explosive free surface.

Computations employing a uniform cell thickness gave velocities of the leading edge of the explosive gas blast of 6.8 km/sec, significantly less than the 8 to 12 km/sec observed. Numerical experiments with an ideal gas equation of state indicate that a variable cell thickness, with a very thin cell thickness as toward the outside edge of the explosive sphere, are required to obtain the theoretical terminal velocity. Using variable cell dimensions such that the outer cells thickness was 10^{-7} to 10^{-6} of the radius the calculated gas blast front velocities of 9.82 and 8.97 km/sec were obtained with a Wilkins equation and an KSZK equation of state. These values are close to the experimental results.

A Wilkins equation of state calculating using a Chapman–Jouguet energy (U_0) of 0.060 mbar/cm^3/cm^3 of original explosive, although giving too low a value for u_f of 6.8 km/sec, describes more closely the observed pressure profiles than a Landau–Stanyukovich–Zeldovich–Kompaneets (LSZK) equation of state. For example, at 38.1 cm from a 0.2-g charge, the Wilkins and LSZK equations gave rise times of 40 and 57 μsec, as compared to $37+10, -7$ μsec which were measured. At 38.1 cm or 122 charge radii from the charge, the reflected pressure level calculated by the Wilkins equation with $U_0 = 0.060$ Mbar is 0.031 bar which agrees fairly well with the measured reflected pressures of 0.021 ± 0.008 bar. At 102 cm or 327 charge radii from the charge, both the LSZK and the Wilkins equation gave good descriptions of the rise time (142 and 159 μsec, respectively) compared to the 170 ± 30 μsec observed. At this distance the calculated reflected pressure levels of ~ 0.003 bar are too high by about a factor of ~ 3 as compared to the measured values of 0.0010 bar. This result suggests that the effective polytropic exponent in these equations of state (both using variable cell widths) give good qualitative descriptions of the observed pressures. Only minor adjustments of the effective polytropic exponent, or perhaps effective explosive mass and/or Chapman–Jouguet energy would be required to fit the experimental data more exactly.

ACKNOWLEDGMENTS

This research was sponsored in part by the National Aeronautics and Space Administration at Stanford Research Institute (SRI) under contract NAS 9-5885, and partially supported by contracts NAS 9-5632 and NGL 05-020-232 to Stanford University and contact NGL 05-002-105 to the California Institute of Technology. The experiments and many of the calculations were performed while the authors were staff members of the Poulter Laboratory at SRI. We appreciate the able computational help of J. O. Erkman, G. M. Muller, and especially D. Gerneth who carried out the results of Table III. We are indebted to D. Stevens who helped with the initial explosive preparation and to R. Goettelman and B. Loo who helped analyze the data.

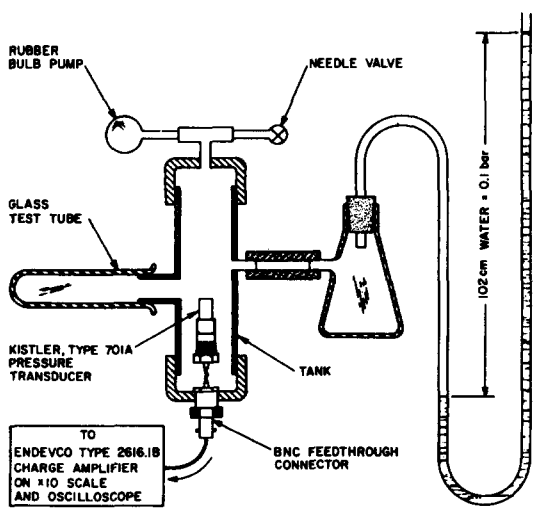

FIG. 11. Experimental arrangement for calibrating Kistler pressure transducer. Air overpressure is brought to desired level (as determined by height of water column) using bulb pump and needle valve. Pressure is reduced suddenly to ambient value by breaking glass test tube.

APPENDIX A: CALIBRATION OF KISTLER PRESSURE TRANSDUCERS

Air was employed as the pressure medium in order to achieve a calibration of the Kistler Type 701A pressure transducer at the low levels (around 0.1 bar) of the present experiments. (The manufacturer's calibrations are carried out at considerably higher pressure levels.) The pressure in a small tank (Fig. 11) induced by a rubber bulb pump is determined from the differential height of a column of water. (The air is saturated with water vapor.) The tank pressure is released by suddenly breaking a glass test tube seal.

The signal generated by the transducer is recorded by oscilloscopes operating in the single-sweep mode, as in the gas blast experiments. The recorded height (see Fig. 12) of the decaying voltage (pressure step) is extrapolated back to zero time to obtain the dynamic voltage (pressure) change. The calibrations obtained were reproducible to $\pm 5\%$ and agreed well with those obtained from the manufacturer.

APPENDIX B: CALIBRATION OF THE MODIFIED CONDENSER MICROPHONE

The response of the modified Bruell and Kjaer 4135 microphone in terms of an absolute dynamic pressure at 250 Hz was obtained using a 2×10^{-5} bar standard pressure source (B&K piston-phone Type 4220). The arrangement of Fig. 13 was employed to obtain the frequency response of the modified microphone relative to that at 250 Hz at atmospheric pressure. The nylon grid allowed electrostatic calibration of the diaphragm to be performed without removing the foam plug. The microphone response was obtained at a series of frequencies generated by an audio oscillator. The oscillator signal voltage electrostatically displaces the diaphragm of the microphone, thus acting similar to sound pressure. The microphone with the electrostatic actuator attached and the cathode follower circuit were placed in a vacuum tank (Fig. 1). The relative frequency response was then obtained at pressures down to 5×10^{-5} Torr. The modified microphone is more sensitive in vacuum than in air by a factor of 3 ± 0.5 and 8 ± 1 between 10 and 25 kHz. This effect arises because the foam plug expands slightly in vacuum and increases the tension in the microphone diaphragm.

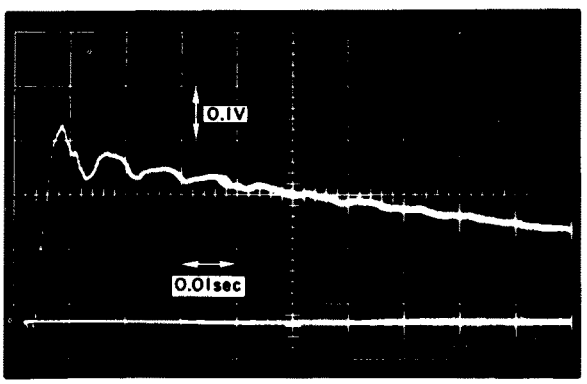

FIG. 12. Typical Kistler pressure transducer calibration record (test 12, oscilloscope 7). Pressure in test chamber is released by breaking test tube seal shown in Fig. 11.

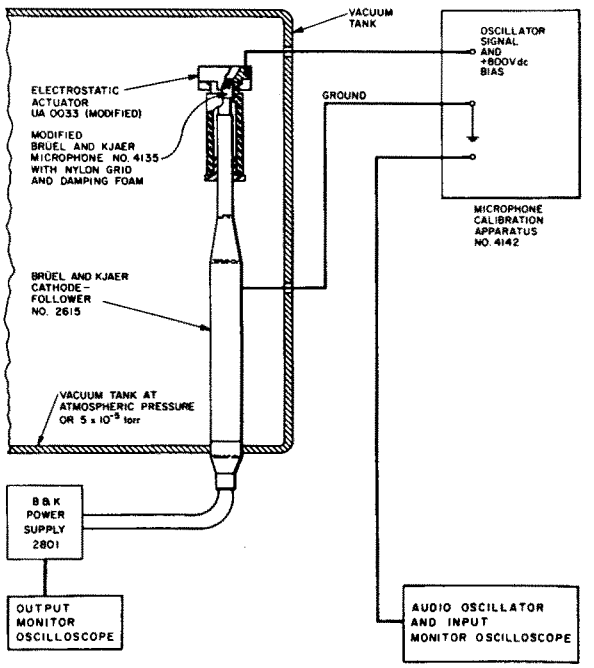

FIG. 13. Experimental arrangement for calibration of modified B&K microphone in hard vacuum.

[1] C. K. Thornhill, Armament Research and Development Establishment Rep. (B) 30/58 (1958).
[2] M. Lutzky, Naval Ordnance Laboratory NOL-TR-62-19 (1962).
[3] K. P. Stanyukovich, *Unsteady Motion of Continuous Media* (Pergamon, London, 1964).
[4] C. Greifinger and J. D. Cole, AIAA J. **3,** 1200 (1965).
[5] H. Mirels and J. F. Mullen, AIAA J. **1,** 596 (1963).
[6] E. H. Wedemeyer, Ballistic Research Lab. Rep. 1273 (1965).
[7] E. W. Hubbard, AIAA J. **5,** 378 (1960).
[8] P. Molmud, Phys. Fluids **3,** 362 (1960).
[9] C. D. Mader, Los Alamos Scientific Lab. Rep. 2900 (1963).
[10] N. Lundborg, *Proceedings of the Fourth Symposium (International) on Detonation,* (ACR-126, U.S. Gov't Printing Office, Washington, 1965), p. 176.
[11] W. H. Jack, Jr., and B. F. Armendt, Ballistics Research Laboratories, BRL Rep. 1280 (1965).
[12] R. L. Kovach and T. J. Ahrens, Geophysics **35,** 33 (1970).
[13] R. F. Fletcher, D. Gerneth, and C. Goodman, AIAA J. **4,** 755 (1966).
[14] Ia. B. Zeldovich and A. S. Kompaneets, *Theory of Detonation* (Academic, New York, 1960).
[15] C. Mader (private communication, 1966).
[16] W. Herrmann, E. A. Witmer, J. H. Percy, and A. H. Jones, M. I. T. Tech. Documentary Rep. ASD-TDR-62-399, 1962.
[17] M. L. Wilkins, Methods of Computational Physics **3,** 211 (1964).
[18] C. Greifinger, private communication (1966).